# Nearly monoenergetic positive ion beam with self-neutralized space charge extracted from a pulsed plasma

**Ya-Ming Chen**[1], **Ryan Sawadichai**[1], **Siyuan Tian**[1,3], **Vincent M Donnelly**[1], **Paul Ruchhoeft**[2] **and Demetre J Economou**[1]

[1] Plasma Processing Laboratory, Department of Chemical and Biomolecular Engineering, University of Houston, Houston, TX 77204, United States of America
[2] Department of Electrical and Computer Engineering, University of Houston, Houston, TX 77204, United States of America

E-mail: vmdonnelly@uh.edu, pruchhoe@central.uh.edu and economou@uh.edu

## Abstract

A nearly monoenergetic $Ar^+$ ion beam (100 eV peak energy, 3.5 eV full width at half maximum), with self-neutralized space charge, was extracted from a power modulated (pulsed) inductively coupled plasma (ICP), through a single grounded grid. The beam energy was set by applying a synchronous DC bias voltage to a boundary electrode in contact with the plasma, in the late afterglow of the power pulse. A retarding field energy analyzer and a movable Faraday cup were used to measure the ion energy distribution (IED) and the time resolved ion and electron current densities, as a function of position along the beam axis, to unravel the mechanism of self-neutralization of the space charge of the beam. When a +100 V DC bias was applied to the boundary electrode during the afterglow, a ~100 eV beam (ion density ~$10^9$ $cm^{-3}$) emerged that was space-charge neutralized by periodic injection of electrons, mainly during the early afterglow, into the region downstream of the extraction grid. A background plasma (electron density ~$10^{10}$ $cm^{-3}$) was formed by these electrons, in conjunction with relatively low-energy ions (1–10 eV) that flew out of the ICP when the DC bias was off, as well as formed by resonant charge exchange of the 100 eV beam ions with the background Ar in the downstream region near the extraction grid. The behavior of the beam IED as a function of pressure and power of the ICP as well as the timing of application of the DC bias voltage was also studied.

Keywords: ion energy distribution, ion beam etching, space charge neutralization

(Some figures may appear in colour only in the online journal)

## 1. Introduction

Ion beams are used extensively for etching and deposition of thin films, ion implantation and surface structuring [1–3]. Specific applications include reactive ion beam etching (RIBE) [4] and ion beam assisted deposition (IBAD) [5]. Furthermore, ion beams find application in ion thrusters [6], ion beam lithography through stencil masks [7] and more recently nanopantography [8, 9]. Many of these applications require high ion flux and well defined ion energy. For example, nanopantography requires a monoenergetic ion beam to create sub-5 nm patterns in a massively parallel manner [10]. To obtain the maximum ion flux and minimum width of the ion energy distribution (IED), effective neutralization of the space charge of the ion beam is necessary, especially for beams with low ion energy and/or high current density [11, 12]. In addition, space charge compensation is required when etching insulators, to avoid surface charging and suppression of the energy of subsequent ions striking the insulator surface.

[3] Currently with Lam Research, Fremont, CA.

Neutralization of the space charge of a positive ion beam requires the injection of electrons. In previous studies [6, 13], hot tungsten filaments were used to thermionically emit electrons to neutralize the space charge. The performance of the neutralizing filaments, however, is restricted by their limited lifetime, system contamination, and the inconvenience of the required extra power supplies. An alternate approach was reported by Dudin *et al* [14] who realized a charge-compensated ion beam using a single radio frequency (RF) biased extraction grid. Rafalskyi and Aanesland [15] applied a RF voltage to a two-grid ion extraction system, through a blocking capacitor, which could result in a space charge neutralized ion beam. These approaches, however, resulted in ion beams with a wide ion energy distribution.

In this work, a self-neutralized, nearly monoenergetic positive ion beam was extracted in the afterglow of a pulsed plasma by applying a synchronous DC bias voltage on a boundary electrode in contact with the plasma. No hot filaments or other external sources of electrons were employed to neutralize the space charge of the beam. A retarding field energy analyzer (RFEA) and a movable Faraday cup were used to investigate the dependence of the IED and ion and electron currents on plasma operating parameters, such as inductively coupled plasma (ICP) source pressure and RF power. Time- and space-resolved electron and ion current density measurements were analyzed to unravel the mechanism of self-neutralization of the beam space charge.

## 2. Methods

### 2.1. Generation of a nearly monoenergetic ion beam

Figure 1 shows a schematic of the experimental system, comprised of an ICP source, an ion drift tube, and a processing chamber [8, 16]. Two-stages of differential pumping maintained pressures in the 28 cm long drift tube and 21 cm long processing chamber, respectively, of $4.6 \times 10^{-6}$ and $1.5 \times 10^{-6}$ Torr at 5 mTorr, and $2.7 \times 10^{-5}$ and $9.0 \times 10^{-6}$ Torr at 35 mTorr in the plasma source, with 5.4 sccm Ar flowing through the source. The base pressures in the drift tube and processing chamber were $1.1 \times 10^{-7}$ and $2.0 \times 10^{-7}$ Torr, respectively, with no gas flow. A technique developed by Xu *et al* [17] was used to extract a nearly monoenergetic ion beam from a power modulated (pulsed) plasma through a grounded metal grid. An Ar ICP was generated in an alumina tube (12.7 cm long, 5.08 cm inside diam.), using a 3-turn copper coil powered at 13.56 MHz (Advanced Energy, model AE Paramount Generator). Using an ICP offered the advantage of more than an order of magnitude higher beam current, compared to the capacitively coupled plasma (CCP) reactor employed in earlier work. This improved the throughput of etching [18] during nanopantography.

A single grounded grid (W mesh with 200 $\mu$m square openings and 84% transparency), henceforth to be referred to as the 'ion extraction grid', covered a 5 mm diameter aperture in one of the flat walls of the cylindrical plasma source. When no voltage is applied to the boundary electrode, the plasma potential, $V_p$, is expected to be ~4.8$T_e$ above ground potential.

Langmuir probe measurements (see below) of the powered and late afterglow (power off) regions yield respective values of 4.5 and 0.2 eV for $T_e$, and 26 and 0.3 V for $V_p$, reasonably close to the expected values. In the afterglow of the pulsed plasma, a synchronized DC bias voltage, $V_{bias}$ was applied on a boundary electrode in contact with the plasma, raising the plasma potential to close to $V_{bias} + V_p$. This caused positive ions to be expelled from the plasma through the extraction grid. In the late afterglow, the plasma potential dropped to near zero, and was set to a value controlled by the applied DC bias, forming a nearly monoenergetic ion beam.

The pulsed-power and synchronous boundary bias voltage timing is shown in figure 2 (referred to throughout as base case conditions). Unless otherwise stated, RF power (800 W peak at 13.56 MHz) to the ICP was modulated at 10 kHz (100 $\mu$s period). The active glow (power-on) commenced at $t = 0$; power was turned off (beginning of the afterglow) at $t = 20$ $\mu$s, (i.e. a duty cycle of 20%). A 100 V DC bias voltage was applied to the boundary electrode 50 $\mu$s into the afterglow ($t = 70$ $\mu$s), lasting 20 $\mu$s. A new cycle started at $t = 100$ $\mu$s. Other base case values included plasma gas pressure = 5.0 mTorr and Ar gas flow rate = 5.4 sccm.

In a few initial experiments, 30 A of current was supplied to an array of four yttria-coated iridium filaments to provide low-energy electrons, to neutralize the positive space charge in the extracted ion beam. These filaments were not in place for all subsequent experiments.

### 2.2. Retarding field energy analyzer

A retarding field energy analyzer (RFEA), installed 80 cm downstream of the extraction grid of the ICP source (figure 1) [10], was used to measure ion energy distributions (IEDs). For each set of operating conditions examined, the ion beam current was found by integrating the corresponding IED. The RFEA was made of a stack of three parallel Ni grids, each with 40 $\mu$m square openings and 85% transparency, spaced 1.5 mm apart from one another, and a stainless steel, grounded current collector, spaced 5 mm from the bottom grid. The top grid was grounded. A 1 Hz, 0 to 120 V sawtooth waveform was applied to the middle (energy selector or discriminator) grid (held on a 5 mm diam. aperture), using a Stanford Research Systems DS345 function generator and an AVTECH AV-112H-PS-UHA high voltage amplifier. The bottom grid was biased with a DC voltage of −20 V to suppress secondary electron emission from the current collector plate. The transparency of the three-grid stack was approximately 60%. A Keithley 6485 pico-ammeter was used to measure the collector current as a function of voltage applied to the middle grid. Data were recorded by an oscilloscope (Agilent Technologies DSO-X 2024A) and smoothed by averaging 1024 current–voltage (*I*–*V*) curves to reduce noise.

### 2.3. Faraday cup

A Faraday cup attached to a magnetic transfer arm was used to measure the time resolved ion and electron currents along the beam axis between 0 and 60 cm from the extraction grid.
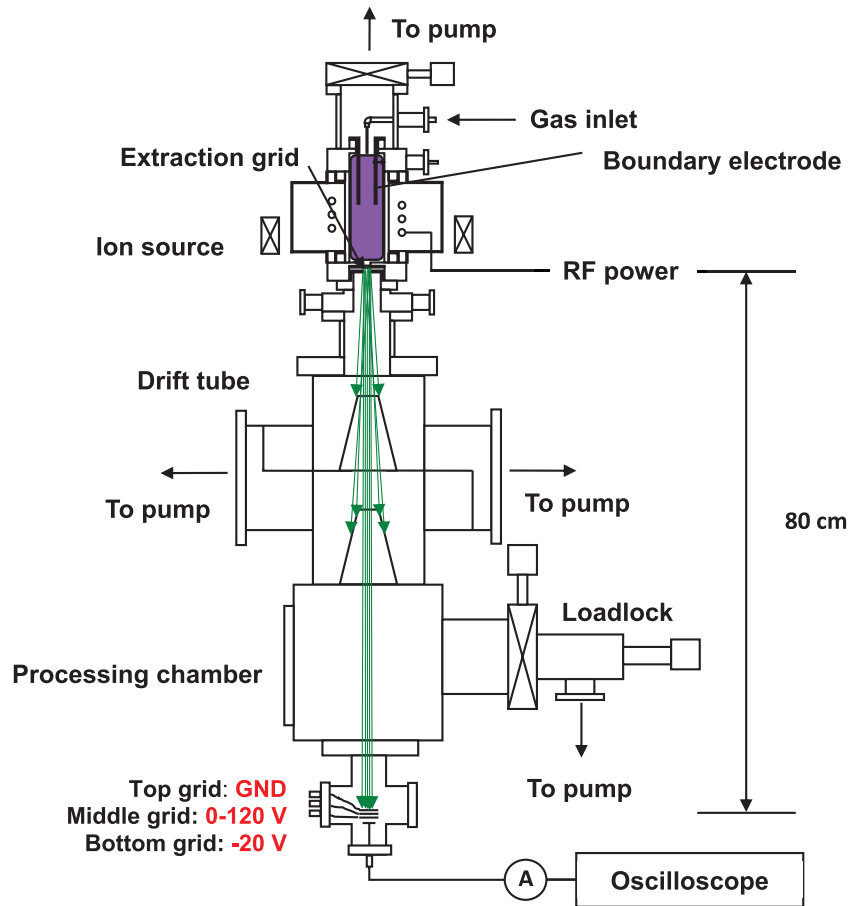
**Figure 1.** Schematic of the experimental setup for ion beam extraction. The retarding field energy analyzer (RFEA) is shown at the bottom of the figure. The distance from the extraction grid to the top, grounded (GND) grid of the RFEA was 80 cm. The ion beam is schematically shown in green arrows.
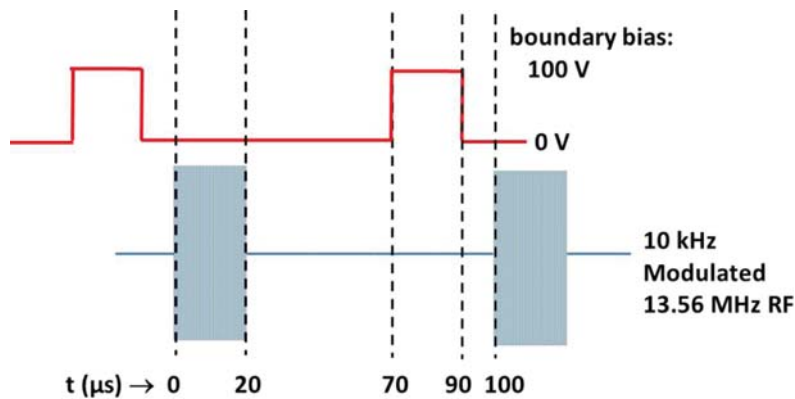


**Figure 2.** Schematic of the pulsed plasma power and bias sequences. 13.56 MHz RF power (800 W peak) was applied to the ICP coil at $t = 0$. At $t = 20$ $\mu$s, the power was turned off to begin the afterglow. At $t = 70$ $\mu$s, a 100 V DC bias was applied to the boundary electrode for 20 $\mu$s. The power and bias modulation frequency was 10 kHz (100 $\mu$s period). The parameter values given here refer to the base case.

The body of the Faraday cup was made of three stainless steel coaxial tubes (figure 3). Kapton tape electrically isolated the inner tube (current collector cup) from the grounded middle tube. The outermost tube (outer sleeve), made electrical contact with the grounded middle tube. Two parallel grids were held by the outer sleeve. A third grid was spot welded to the front of the current collector cup. The grids were made of Ni mesh with 40 $\mu$m square openings and 85% transparency. A Teflon disc behind the current collector cup electrically isolated the cup from mechanical supports of the device. The current collector cup was connected to a Kapton-coated wire that was input to a current amplifier (Keithley model
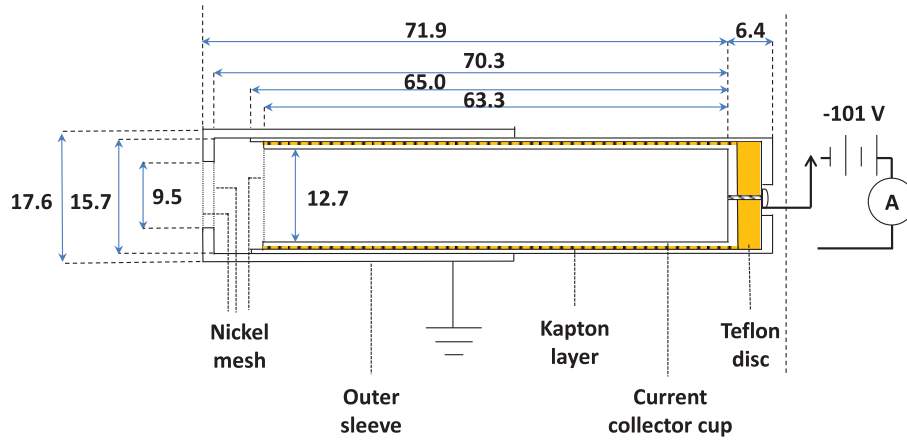
**Figure 3.** Schematic of the Faraday cup used for space- and time-resolved current measurements along the beam axis. The dimensions are in mm.

427 pico-ammeter) either directly, or biased at $-101$ V with batteries. The direct connection measured the net current, while the negatively biased connection repelled the electrons and provided just the positive ion current. Electron current was determined by subtracting the ion current from the net current. Time resolved measurements of these currents were obtained by recording the pico-ammeter signal with an oscilloscope (Agilent Technologies DSO-X 2024A) and smoothed by averaging 1024 measurements to reduce noise.

*2.4. Langmuir probe*

A Langmuir probe (Scientific Systems Smartprobe) was used to characterize the ICP source. A 0.2 mm diam. tungsten wire, covered by a 0.5 mm O.D. alumina tube, was used for the probe tip, with a length of 4 mm exposed to the plasma. Time resolved electron temperature and electron density were measured by positioning the tip at different axial locations inside the ICP source, from the center to the edge of the source (2 cm away from the extraction grid). The probe modifications and procedures to extract electron energy distribution functions and electron temperatures as well as number densities from current–voltage characteristics are described in detail elsewhere [19, 20].

## 3. Results and discussion

As mentioned above, the pulsed plasma source can produce an energy-selectable, nearly monoenergetic ion beam without the need for hot filaments to neutralize the space charge [21]. This apparently occurs because of periodic injection of electrons into the region downstream of the extraction grid. This 'self-neutralization' of space charge is dramatically demonstrated in figure 4, which shows the ion beam current measured 80 cm from the extraction grid, for continuous wave (cw) plasma (black), and pulsed plasma (red). For cw plasma, the ion beam current is negligible without any electron emitting filaments (i.e. at zero filament current), and increases substantially when electron emitting filaments were used (i.e. at 30 A filament
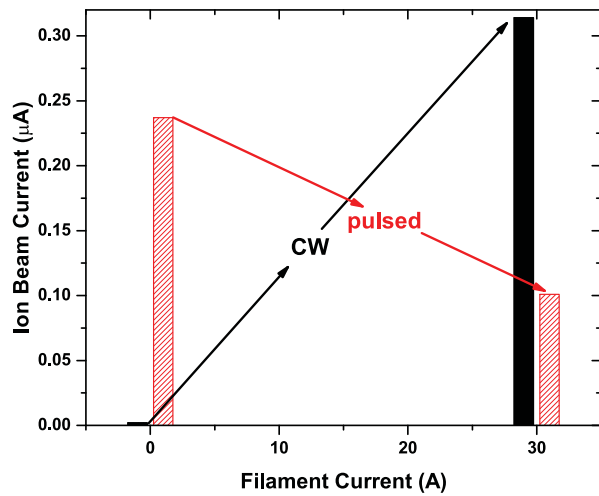


**Figure 4.** Ion beam current measured 80 cm from the extraction grid with the RFEA, for 300 W continuous wave (cw) plasma or 500 W (on power), 15% duty cycle pulsed plasma. A continuous 40 V boundary electrode bias was applied in the cw case, while in the pulsed plasma, a synchronous 100 V DC bias was applied to the boundary electrode, 15 $\mu$s into the afterglow.

current). Thus as expected, an external supply of electrons is necessary in a cw plasma to neutralize the space charge of the ion beam, preventing coulomb collisions from causing excessive divergence of the beam as it propagates downstream. The situation is very different in the case of pulsed plasmas. In this case, a substantial ion beam current was measured even without any filaments (i.e. at zero filament current). In fact, turning the electron emitting filaments on resulted in lower ion beam current. Apparently, in the case of pulsed plasma, electrons from the plasma itself neutralize the ion beam space charge (self-neutralization). No external source of electrons is needed. It turns out that, at zero filament current, the ion beam current extracted from the pulsed plasma is 120X the ion beam current extracted from the cw plasma. The purpose of the present study is to characterize the positive ion beam as a function of plasma source operating conditions and gain
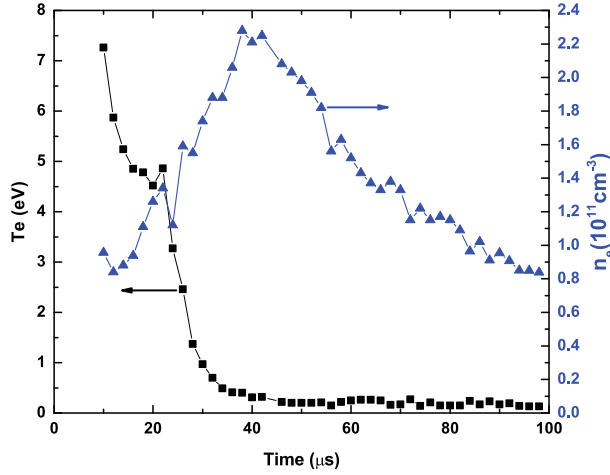
**Figure 5.** Time resolved electron temperature ($T_e$) and electron density ($n_e$) measured by a Langmuir probe in the afterglow of a pulsed Ar plasma at the edge of the reactor, 2 cm upstream from the extraction grid. No boundary bias was applied in these experiments. Base case plasma operating conditions were used.

insights into the mechanism of space charge neutralization of the beam extracted from pulsed plasmas.

### 3.1. Plasma source characterization

Langmuir probe measurements of electron number density and temperature at the edge of the plasma source, 2 cm upstream of the extraction grid, are presented in figure 5. As expected, $T_e$ spikes at the beginning of the power-on period before reaching 4.5 eV, when the electron density is about $1.3 \times 10^{11}$ cm$^{-3}$ at the time the power is turned off at $t = 20$ $\mu$s. The flux of ions passing through the grid is given by

$$\Gamma = 0.6 n_0 T_{\text{grid}} v_B \tag{1}$$

where $n_0$ is the ion density (equals $n_e$) near the edge of the plasma, $v_B$ is the Bohm velocity and $T_{\text{grid}}$ (=0.84) is the fraction of open area (i.e. transmission) of the extraction grid. This flux does not depend on the boundary bias voltage. Using the data in figure 5, the ion flux as a function of time, computed from equation (1), is given in figure 6.

During the late activeglow (power-on), the electron density and temperature at the plasma edge (near the grid) were $n_e = 1.3 \times 10^{11}$ cm$^{-3}$ and $T_e = 4.5$ eV (figure 5). These values yield a Debye length, $\lambda_D = 44$ $\mu$m. Near the end of the afterglow, $n_e = 1.0 \times 10^{11}$ cm$^{-3}$, $T_e \approx 0.2$ eV, and $\lambda_D \approx 10$ $\mu$m. The Child law sheath thickness is estimated using:

$$s = \frac{\sqrt{2}}{3} \left( \frac{2 V_{\text{sh}}}{T_e} \right)^{0.75} \lambda_D \tag{2}$$

where $V_{\text{sh}}$ is the voltage of the sheath over the upstream side of the extraction grid, and $T_e$ is expressed in V. For the low energy ions produced during the activeglow, $V_{\text{sh}} = 4.8 T_e$ and s ~110 $\mu$m, while for the high energy ions ($V_{\text{sh}} = 100$ V and $T_e = 0.2$ V), the sheath thickness is s ~800 $\mu$m.

Without plasma molding (i.e. penetration and bending of the electric field in the hole) [22], Ar$^+$ will exit the grid holes
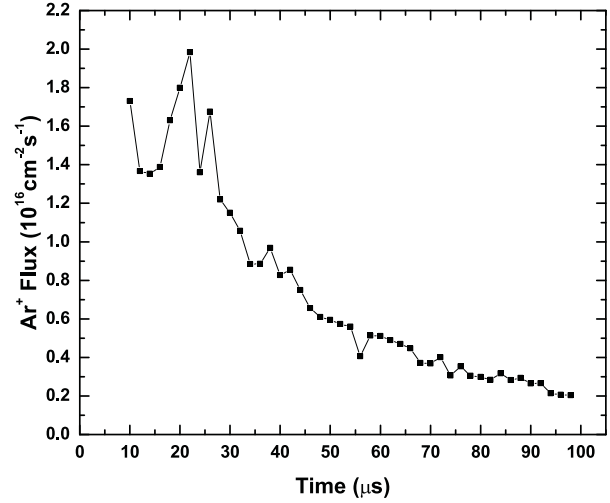


**Figure 6.** Ar$^+$ flux passing through the extraction grid, determined from equation (1) and the data in figure 5.
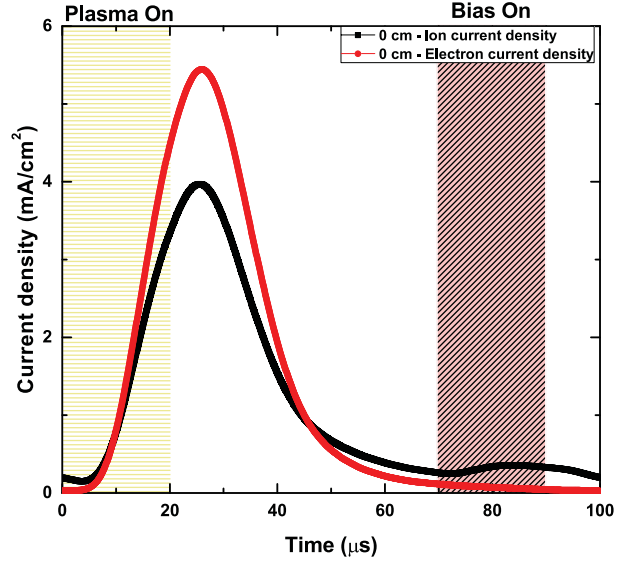


**Figure 7.** Time-resolved ion and electron current densities measured with the Faraday cup placed <1 mm downstream of the extraction grid. Base conditions were used.

with angles determined by the vector sum of the directed velocity through the sheath and the isotropic velocity of ions in the pre-sheath. The average divergence angle, $\theta_{\text{av}}$, is therefore

$$\theta_{\text{av}} \approx \arctan \left( \frac{v_P}{v_D} \right) \tag{3}$$

where $v_P$ is the average projection on the plane of the sheath of the isotropic distribution of velocities of ions in the pre-sheath with kinetic energy $T_e/2$, moving toward the sheath edge ($v_P$ cm s$^{-1} = 1.4 \times 10^6 [\cos 45°] \sqrt{\frac{T_e}{2m}}$), and $v_D$ is the directed velocity perpendicular to the sheath plane for ions that are accelerated toward the grid by the sheath potential. Without bias, $v_D = 1.4 \times 10^6 \sqrt{\frac{4.8 T_e}{m}}$, with $4.8 T_e$ being the argon plasma potential with respect to the grounded
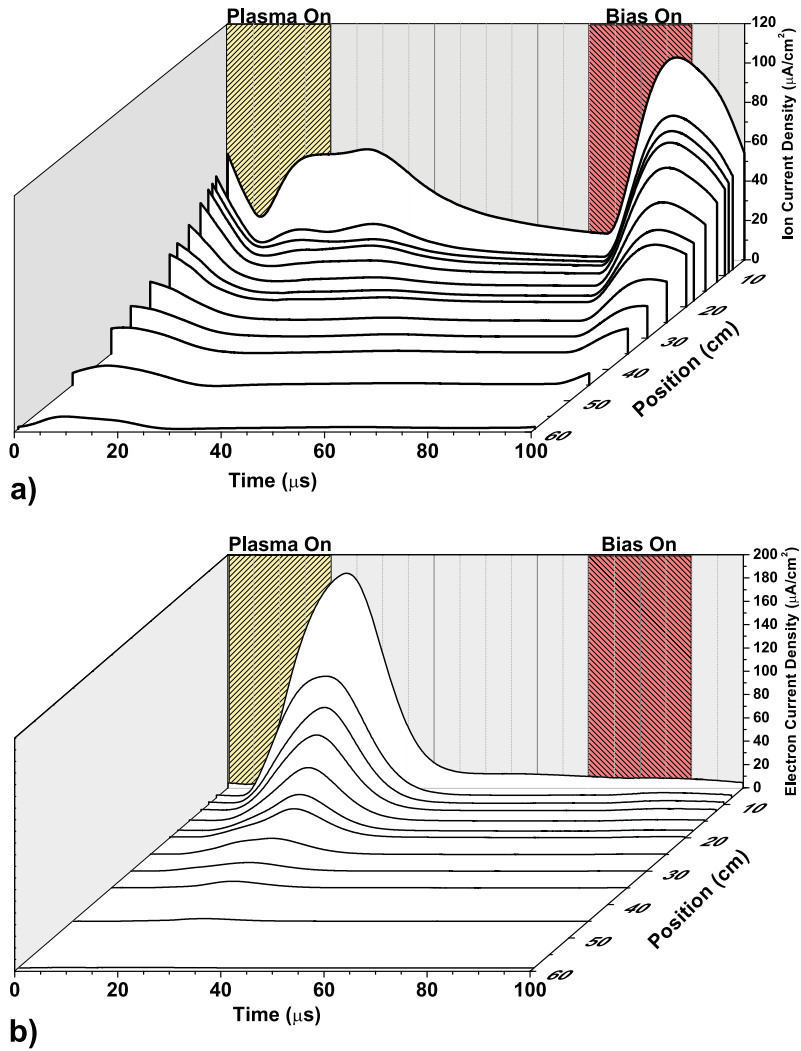
**Figure 8.** Time- and space-resolved measurements of (a) ion current and (b) electron current densities along the beam axis (5–60 cm away from the extraction grid). Base conditions were used.

grid. In the above formulas, $T_e$ is in eV, and $m$ is the atomic mass of the ion ($m = 40$ for Ar). Equation (3) yields $\theta_{av} \approx \arctan\left(\frac{0.707}{\sqrt{2 \times 4.8}}\right) = 13°$. When the 100 V boundary bias voltage was turned on in the afterglow (where $T_e = 0.2\,\text{eV}$ hence $v_P = 6.9 \times 10^4$ cm s$^{-1}$), the plasma potential quickly rose to this value. Positive ions were accelerated from the plasma potential across the sheath adjacent to the grounded extraction grid, leading to $v_D = 2.2 \times 10^6$ cm s$^{-1}$ and $\theta_{av} = 2°$ from equation (3).

Previous measurements in an ICP from our lab [23, 24] showed that for Ar$^+$ accelerated across a sheath of thickness $s$ and passing through a single hole of diameter $d$, the angular spread was constant for $d/s < 0.4$ and therefore dominated by the thermal velocity component of ions entering the sheath (no plasma molding). For the 100 eV ion beam generated by the biased, afterglow plasma, $d/s = 0.25$ and the energy spread should be dominated by the ion thermal velocity distribution,

which from equation (3) is ~2°. When the $d/s$ ratio exceeds 1, the angular spread of ions due to plasma molding becomes substantial. For the activeglow with bias off, $d/s = 1.8$ in our system, and plasma molding will contribute substantially to the angular spread of the low-energy ions leaving the grid.

### 3.2. Time- and space-resolved measurements of ion and electron current density

Time-resolved measurements of ion and electron current densities are shown in figure 7 when the Faraday cup was nearly touching the extraction grid (from the downstream side). The ion current density consists of two components: a relatively intense feature peaking at about 6 $\mu$s after the end of the power-on period, and a weaker feature peaking after the initiation of bias voltage (100 V DC) on the boundary electrode (bias on). An estimate of the time at which the ion current density reaches its peak value, accounting for the flight time

of ions from the extraction grid to the Faraday cup, is given in appendix A.

About 20 $\mu$s into the afterglow, $n_e$ ~$2 \times 10^{11}$ cm$^{-3}$ and $T_e$ has fallen to ~0.2 eV (figure 5). Assuming a sheath potential of $4.8T_e = $ ~1 eV, $v_D = 2.2 \times 10^5$ cm s$^{-1}$. This corresponds to a maximum delay in detection of these very low energy ions of ~35 $\mu$s, for the unbiased current collector cup. Given the angular spread, this is probably closer to ~20 $\mu$s. For the biased collector, the delay is ~15 $\mu$s. These time delays, in addition to charge exchange, lead to considerable broadening of the tailing ion current in figure 7, relative to that expected from the flux leaving the plasma shown in figure 6.

If we use the $T_e$ and $n_0$ values of 4.5 eV and $1.3 \times 10^{11}$ cm$^{-3}$ near the end of the power-on period (figure 5), then the peak value of the low energy ion flux from equation (1) is $\Gamma_{l+} = 1.9 \times 10^{16}$ cm$^{-2}$ s$^{-1}$, corresponding to a current density of 3.0 mA cm$^{-2}$. This is in reasonable agreement with the measured peak value of 1.8 mA cm$^{-2}$ in figure 7. The number density of low energy ions in the downstream volume close to the grid is simply $n_{l+} = \Gamma_{l+}/v_D$, where $v_D$ is for acceleration across the $4.8T_e$ plasma sheath potential. At the end of the power-on period, $T_e = 4.5$ eV and $v_D = 1.0 \times 10^6$ cm s$^{-1}$. Using the estimated peak flux of $\Gamma_{l+} = 1.9 \times 10^{16}$ cm$^{-2}$ s$^{-1}$ adjacent to the grid, yields $n_{l+} = 1.9 \times 10^{10}$ cm$^{-3}$. Near the end of the afterglow, when $T_e = 0.2$ eV (figure 5), $v_D = 2.2 \times 10^5$ cm s$^{-1}$, $n_0 = 1 \times 10^{11}$ cm$^{-3}$, $\Gamma = 3.5 \times 10^{15}$ cm$^{-2}$ s$^{-1}$ from equation (1), and thus $n_{l+} = 1.6 \times 10^{10}$ cm$^{-3}$. Hence the average $n_{l+}$ of low energy ions just downstream of the grid has a nearly constant value of $1.8 \times 10^{10}$ cm$^{-3}$. At this high number density, the plasma is quasi-neutral (see discussion below), so ambipolar diffusion implies equal electron and ion currents, as is approximately the case in figure 7.

When the boundary bias voltage is turned on at $t = $ 70–90 $\mu$s (i.e. 50–70 $\mu$s after cessation of ICP power—figure 2), the flux from the plasma source has dropped ~6-fold (figure 6), reasonably close to the ten-fold drop in ion flux measured by the Faraday cup (figure 7). Equating the flux of $3 \times 10^{15}$ cm$^{-2}$ s$^{-1}$ predicted from equation (1) at $T_e = 0.2$ eV and $n_0 = 1 \times 10^{11}$ cm$^{-3}$ with the beam flux, $\Gamma_{b+}$, the ion number density in the high energy ion beam, $n_{b+} = \Gamma_{b+}/v_D$, is ~$1.5 \times 10^9$ cm$^{-3}$ near the peak in figure 7, where we used $v_D = 2.2 \times 10^6$ cm s$^{-1}$ for the 100 eV ions. Electrons cannot escape the ICP source when the plasma potential is raised to 100 V by the application of bias on the boundary electrode. The small electron current that is detected coincident with the arrival of the ion beam in the Faraday cup (figure 7) is left from the previous injection of plasma with the bias off.

Time and space-resolved measurements of the ion and electron current densities were performed along the beam axis using the Faraday cup. Measurements between 5 and 60 cm from the extraction grid are shown in figure 8. As with the measurement close to the grid (figure 7), the ion current density contains a peak appearing shortly after the application of DC bias on the boundary electrode, corresponding to the nominal 100 eV ion beam, and a broad feature (perhaps bimodal) appearing after plasma power is turned on, due to low energy ions.
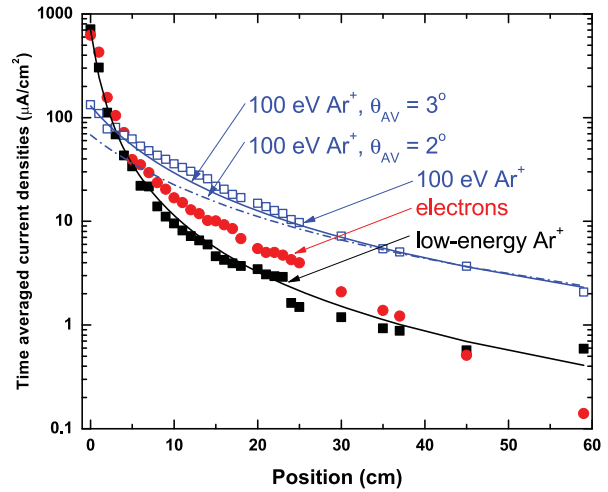


**Figure 9.** Measured ion (blue open squares and solid black squares) and electron (red solid circles) current densities, averaged over one pulse period, as a function of distance from the extraction grid. The lines are ion current densities expected for average divergence angles of 2° and 3° (dash-dot and solid blue lines, respectively) for the 100 eV beam, and 18° (for the low energy ions, solid black line). Base conditions were used.

The high energy (100 eV bias on) ion beam current density was obtained by integrating over the corresponding peak in figure 8(a). The low-energy (bias off) background ion current density was found by subtracting the high energy ion beam current density from the total ion current density integrated over one pulse period. These current densities are plotted in figure 9 (black squares) as a function of distance from the extraction grid between 0 and 60 cm (0–4 cm data are not shown in figure 8), along with the time-averaged electron current densities (from integration of curves in figure 8(b), red solid circles). In the first 4 cm, low-energy ion current densities decay rapidly with distance, while the high-energy peak declines more slowly. Between ~8 cm and ~35 cm, the electron current density is about twice the ion current density. Between ~40 cm and 60 cm, the electron current density drops more rapidly than the ion current density.

The fall-off in ion and electron currents as a function of distance from the grid is a complex, space and time-dependent phenomenon, spanning microns to meter length and ~10 to 500 $\mu$s time scales. Ion beamlets passing through each hole in the square array grid interact with each other in the first few 100 $\mu$m distance from the grid. Simulation of such conditions would be very challenging, and likely would require a full 3D PIC treatment of the near-grid region. Such a treatment is beyond the scope of this experimental study. It is instructive, however, to evaluate some simple scaling concepts.

For example, the initial angular spread in ions emerging from the grid that will contribute to the fall-off in fluxes as a function of distance can easily be estimated. Using a simple approximation to the divergence of the ion beam, $(d_F/[d_F + 2z \tan \theta_{av}])^2$, where $z$ is distance along the axis ($z = 0$ at the extraction grid) and $d_F$ is the diameter of the Faraday cup ($\approx$diameter of the gridded aperture on the plasma
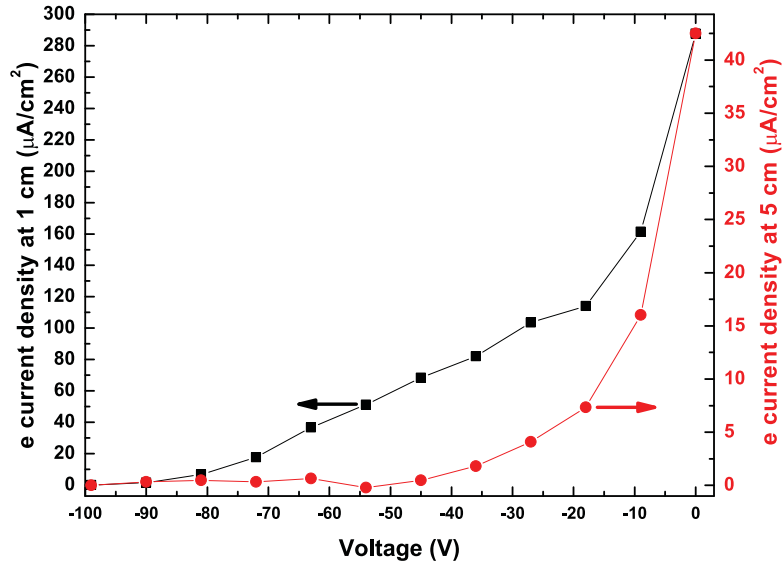
**Figure 10.** Electron current densities as a function of the negative potential applied to the Faraday cup current collector at distances of 1 and 5 cm from the extraction grid. Base conditions were used.

source), the curves in figure 9 were generated. Values for $\theta_{av}$ were computed from equation (3), and also were varied to best fit the measured fall-off in ion currents. The black solid line, normalized to match the low-energy ion current at 0 cm, best reproduces the measurements for $\theta_{av} = 18°$. The added spread, compared to $\theta_{av} = 13°$ computed from equation (3) seems reasonable in view of the expected contribution of plasma molding.

The dash-dot blue line represents the trend predicted for $\theta_{av} = 2°$ computed from equation (3), while the solid blue line represents the 'best fit' for $\theta_{av} = 3°$. Both curves fit the distance dependence of the 100 eV beam beyond 20 cm, when the beam diameter is much larger than the Faraday cup aperture and fluxes approach a fall-off as the reciprocal of distance squared. It is likely that some of the discrepancies between the measured and computed flux for $\theta_{av}$ values due just to thermal spread (i.e. from equation (3)) are due to charge exchange collisions with the background Ar near the grid (see appendix B). Thus the drop off in intensity of both the 100 eV beam and the low energy ions appears to be mainly explained by the initial angular spread of ions emerging from the ICP, combined with charge exchange just past the grid.

It takes about 25 μs for the 100 eV ion beam to travel the 55 cm distance between the extrema of measurements (5 and 60 cm) displayed in figure 8(a). This is within the uncertainty of the expected flight time for this energy (24 μs). Between 5 and 30 cm, the observed flight time of the low energy ions is ~30 μs, consistent with the expected flight time for low-energy ions emerging near the end of the power-on period. Ions leaving the plasma late in the afterglow period will take ~100 μs to travel 25 cm, and ~240 μs to traverse 60 cm. The pulse period is only 100 μs, thus there are 2 or 3 of these 'plugs' present along the beam transport path at any given time, leading to the small observed ion current at all times.

A major peak in electron current density (figures 7 and 8) occurs at 25 μs near the grid, coincident with the peak in low-energy ion current density. A weaker background electron current is present at <35 cm from the grid (barely visible in figures 7 and 8). The main peak in electron current density monotonically shortens to 21 μs as the Faraday cup is moved from 0 to 9 cm, and then stays at $21 \pm 1$ μs all the way to 60 cm. Since the low-energy ion peak moves to monotonically longer delays away from the grid, the electrons near their peak, farther from the grid are coming mainly from the quasi-neutral population of electrons and low-energy ions near the grid, produced near the end of the power-on period. These electrons need a minimum kinetic energy of 1 eV to traverse 60 cm in < 1 μs.

Electrons that escape the plasma during the power-on period must overcome a repelling sheath potential of about 20 V. Therefore, they are expected to have rather low energies after passing through the grid. It appears, however, that the electrons have kinetic energies well in excess of 1 eV. Time-resolved measurements of electron currents were performed at 1 and 5 cm from the grid as a function of negative potential on the Faraday cup. Time-integrated electron current densities are plotted in figure 10. At a distance of 5 cm from the grid, −9 V is sufficient to repel about 2/3 of the electrons. The remaining 1/3 appear to have a distribution of energy that require up to −40 V to repel. At 1 cm, even higher energy electrons are present, requiring nearly −100 V to repel. If we take the second derivative of the electron current density measurements in figure 10 at 5 cm we can extract an 'electron temperature' of ~8 eV, which corresponds to an electron speed of $1.8 \times 10^8$ cm s$^{-1}$, or 200-times larger than the low-energy ions produced at the end of the power-on period. While electrons will be re-accelerated on passing through the sheath adjacent to the downstream side of the grid, they ultimately arrive at the grounded Faraday cup with the energy they had as they
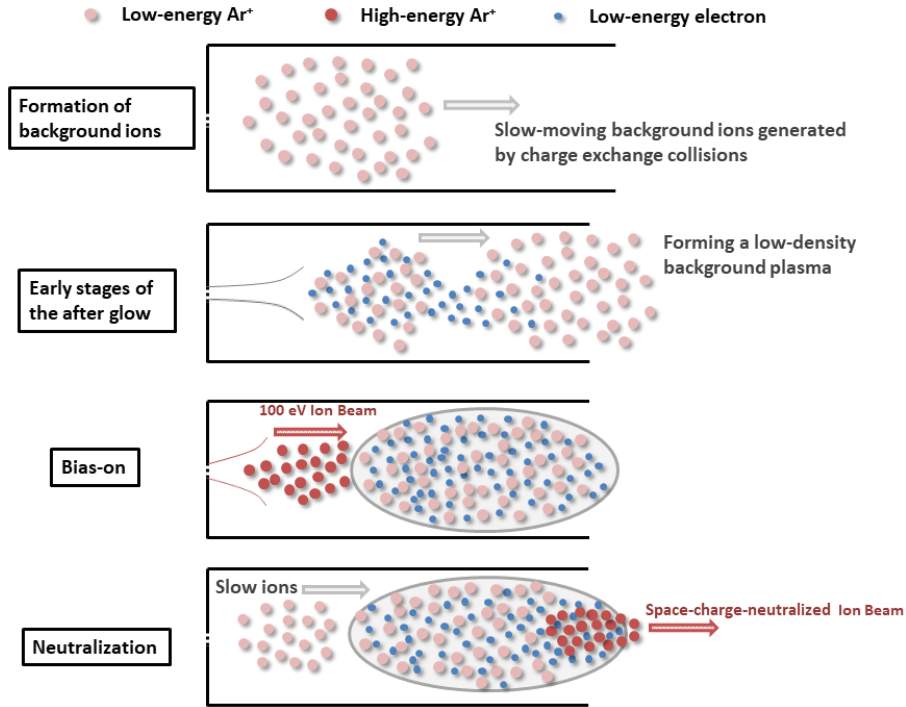
**Figure 11.** Illustration of the mechanism for self-neutralization of the space charge of the positive ion beam.

passed through the grid. Electron–electron collisions would produce a higher energy tail in their energy distribution, but it appears that the electron density in the downstream plasma is insufficient for e–e collisions to produce the observed high energy electrons.

Simulations of the injection of a high energy ion beam into a cold plasma have been reported by Hara *et al* [25] Electron heating due to a two-stream instability was found. The ion beam velocity in their studies was $1 \times 10^9$ cm s$^{-1}$, i.e. much higher than in the present case. With the very high energy ion beam, they found that the electrons achieved velocities as high as $2 \times 10^9$ cm s$^{-1}$ above the ion beam velocity. Even if the $2 \times 10^6$ cm s$^{-1}$ ion beam in the present study produced electrons with ten times this velocity, the electron energy would be of the order of 0.1 eV. Thus, it seems that such two-stream instability is unlikely to be the reason of the observed high energy electrons. As mentioned above, to further study the collective behavior of the ion beam and electrons, a full 3D PIC-MCC simulation would be required, which is beyond the scope of this experimental study.

We now propose a mechanism for self-neutralization of space charge of the ion beam extracted from a pulsed plasma, illustrated in figure 11. As the 100 eV fast ion beam emerges from the extraction grid, after application of a DC bias voltage on the boundary electrode late in the afterglow, the beam traverses the background plasma volume that formed from the prior pulse(s) of ICP power and early afterglow. The beam attracts electrons that neutralize the ion beam positive space charge.

As estimated above, the peak ion density of the 100 eV beam is about $1.5 \times 10^9$ cm$^{-3}$ near the grid, and the nearly constant density of low energy ions is $1.6 \times 10^{10}$ cm$^{-3}$.

Ignoring the high-energy component, and assuming that the plasma into which the ion beam is injected has an electron temperature of ~0.1 eV, yields $\lambda_D$ ~ 20 $\mu$m. If, on the other hand, $T_e = 8$ eV, then $\lambda_D$ ~ 170 $\mu$m. In either case, this is much smaller than the 5 mm diameter of the beam close to the grid, hence the ion beam should be quasi-neutral, consistent with the nearly equal average ion and electron density near the grid (figure 9, at 0 cm). Moving away from the grid, ions that do not suffer charge exchange are only lost from the beam volume in the forward direction toward the face of the Faraday cup, while electrons, which are expected to have a much larger angular spread, can escape in all directions. Hence it is expected that the electron current detected by the Faraday cup will fall below the detected ion current as we move farther from the grid. However, as long as the Debye length corresponding to the plasma formed by the drifting low-energy ions (i.e. when the high energy beam is not present) is smaller than the beam and Faraday cup dimension, charge neutrality is still maintained. At a distance of about 35 cm from the grid, the electron current in figure 9 drops rapidly. At this distance, the low-energy positive ion number density is ~$2 \times 10^7$ cm$^{-3}$. If $T_e$ ~ 8 eV, then $\lambda_D$ ~ 5 mm, or about the aperture radius of the Faraday cup. This implies that electroneutrality breaks down, hence rapid loss of electrons (by free diffusion) is expected at this point (providing $T_e$ is closer to 8 eV than 0.1 eV). Beyond 35 cm, the 100 eV ion beam number density is also low (<$5 \times 10^7$ cm$^{-3}$), hence the total positive space charge is too low to cause much additional divergence of the ion beam.

This neutralization process is similar to that in previous studies in which a separate background plasma was generated in the beam transport path, to neutralize a highly energetic beam in a heavy-ion fusion system [26, 27]. In the present
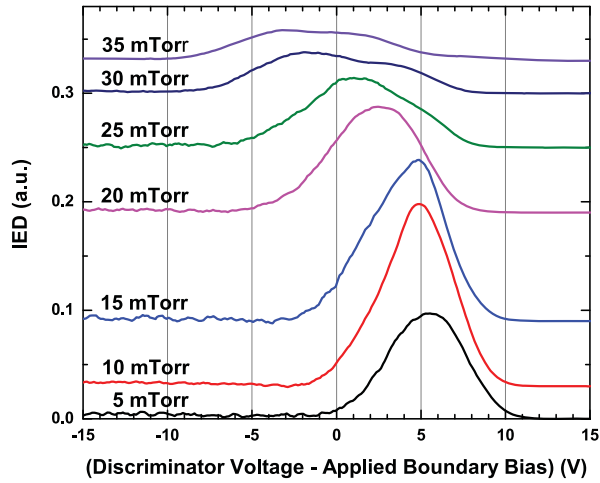
**Figure 12.** Ion energy distributions measured with the RFEA under different pressures (5–35 mTorr) of the ICP source. Otherwise, base conditions were used.

**Figure 13.** IEDs measured at different times (43–65 $\mu$s) after the boundary bias voltage (100 V DC) was turned off in the afterglow (at $t = 90$ $\mu$s, see figure 2). Base conditions were used.

work, instead of generating a background plasma with a secondary plasma source, a plasma is generated naturally by periodic injection of low energy electrons that leave the plasma source in the early afterglow into the volume of low energy ions produced by the unbiased ICP and by charge exchange collisions (of the high energy ions with the background gas) near the extraction grid.

The number of electrons required to neutralize the ion beam per pulse period can be estimated from the fluxes in figure 6. During the period when the bias is off (0–70 and 90–100 $\mu$s) the number of electrons exiting the extraction grid equals the number of positive ions, then this corresponds to $7.3 \times 10^{11}$ electrons. The number of ions in the 100 eV beam exiting the grid between 70 and 90 $\mu$s is $6 \times 10^{10}$ (again from figure 6) and of these roughly 1/3 traverse the first 5 cm without suffering charge exchange (see appendix B) for the base case (ICP pressure = 5 mTorr), hence the number of electrons in the downstream plasma is ~35 times more than required to neutralize the 100 eV beam space charge.

### 3.3. Ion energy distributions at the RFEA position

A distribution of ion energies can be due to: (a) the applied boundary voltage is not absolutely flat, (b) density gradients in the plasma make the energy of ions dependent on the ion's starting point in the plasma, and (c) ion-neutral collisions, especially near the grid, spread the ion energy. Figure 12 shows ion energy distributions measured by the RFEA, at a distance of 80 cm from the extraction grid, as a function of pressure in the plasma source. Between 5 and 20 mTorr, the IEDs consist of a single peak that maximizes at 5.5 eV above the applied bias voltage at 5 mTorr, and decreases monotonically to 2.5 eV above the bias voltage at 20 mTorr. The average energy continues to slowly decrease between 20 and 35 mTorr, while a bimodal distribution begins to be apparent, with components peaking at ~2 eV above and ~3 eV below
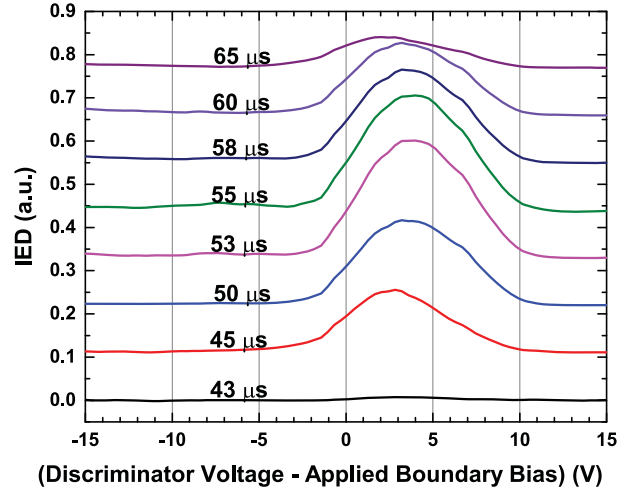
the applied bias voltage. The full width at half maximum (FWHM) of the IEDs (obtained by fitting a Gaussian distribution to the IED and noting the width of the distribution at half the peak height) range from 4.5 eV at 5 mTorr to 7.5 eV at 35 mTorr. The ion beam current (found by integrating the IEDs between 90 and 110 eV) peaks broadly between 10 and 15 mTorr due to the increase in source plasma density, and then falls off with increasing pressure, most likely due to the increasing probability for symmetric charge exchange in the first few cm downstream of the grid [28] (see appendix B).

Pressure in the ICP source can affect the width and peak ion energy of the IED. $T_e$ in the late afterglow has been measured in a somewhat larger ICP system [29]. $T_e$ was found to increase with increasing pressure from ~0.2 eV at 7 mTorr to ~0.5 eV at 50 mTorr. Roughly five times this energy adds to the boundary voltage in determining the sheath potential. $T_e$ in the smaller plasma source used here could perhaps be twice the above values. Consequently, we expect the ion beam for 5 mTorr to peak at ~2 eV above the bias voltage, not 5.5 eV. The 3 V discrepancy is probably due to the combined uncertainty in the voltage settings, measurements of voltages and ground potentials in the plasma source and RFEA.

Some drop in the peak ion beam energy at high pressure is expected due to the larger drop off in charge density between the boundary electrode that is immersed in the high density region of the plasma and the sheath edge at the extraction grid. This results in a fall-off in the plasma potential between the boundary electrode and the grid, in accordance with the Boltzmann relation:

$$\Phi = \ln \left( n_{\text{center}}/n_{\text{edge}} \right) T_e \qquad (4)$$

where $n_{\text{center}}$ is the plasma density at the center of the plasma source, $n_{\text{edge}}$ is the plasma density at the edge of the plasma source, $\Phi$ is the potential drop between the center and edge of the source, $T_e$ is the electron temperature (expressed in V) at $t = 70$ $\mu$s into the afterglow. Given the expected rise in
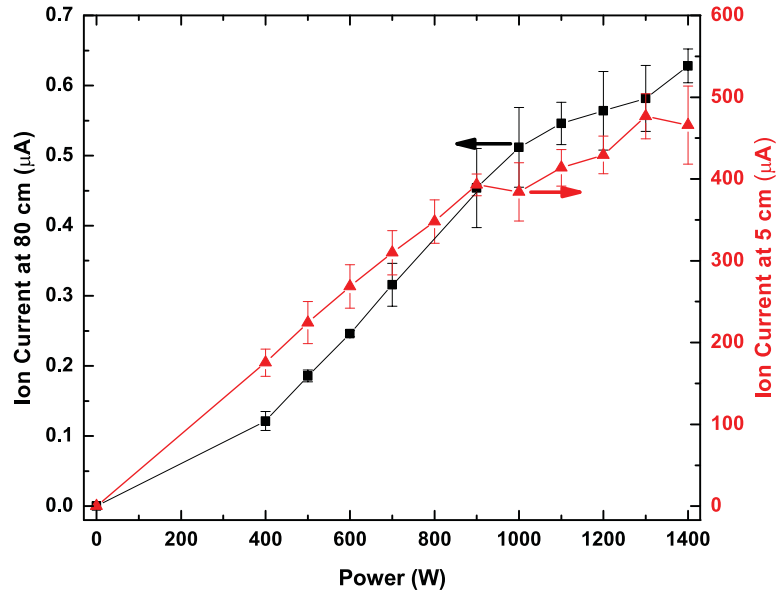
**Figure 14.** The peak ion current of the 100 eV beam, measured using the Faraday cup at 5 cm and the RFEA at 80 cm away from the extraction grid, versus peak RF power to the ICP source. Otherwise, base conditions were used.

both $T_e$ and $n_{center}/n_{edge}$ between 5 and 35 mTorr, this effect could account for perhaps half of the 7 eV drop off in peak ion energy.

Ion collisions with neutrals in the pre-sheath would result in the loss of at most $T_e/2$ and hence $< 1$ eV in the extracted beam energy. Charge exchange collisions only produce very low energy ions. Energy-lowering collisions of ions traversing the ~100 $\mu$m wide sheath adjacent to the grid are infrequent, even at the highest pressure studied. The most likely explanation for the small reduction in energy at higher pressures is highly forward scattering of ions in the beam as it passes through the Ar gas in the first few cm on the downstream side of the grid.

Time resolved IED measurements using the RFEA were also carried out. Figure 13 presents IEDs measured 40–65 $\mu$s after the boundary bias was turned on in the afterglow. Ar ions with energy of 103 eV, require ~43 $\mu$s to travel from the extraction grid to the collector of the RFEA. Indeed, figure 13 shows that at 45 $\mu$s the first ions arrive. These are the ions leaving the plasma at the leading edge of the applied DC pulse. The ion flux continues for the next 20 $\mu$s corresponding to the duration of the applied DC bias. The peak ion energy is nearly constant between 50 and 60 $\mu$s, and slightly lower (2 and 1 eV, respectively) at the beginning and end of the beam arrival. The FWHM of the IED is nearly independent of time.

### 3.4. Power effects

The relationship between RF power input to the ICP source and ion current measured by the RFEA was also investigated (figure 14). The ion current increases nearly linearly with peak RF power between 400 W and 800 W, as expected for an ICP source. Above 800 W, the ion current continues to increase at a slightly less than linear rate at far field (i.e. 80 cm) and

somewhat less than that at 5 cm. The peak ion energy at 80 cm increases from 0.8 eV above the bias voltage at 400 W to 4.6 eV above the bias voltage at 800 W and then reaches a plateau at ~4.8 eV above the bias voltage beyond 800 W (figure 15). The plasma potential measured 50 $\mu$s into the afterglow did not increase appreciably with increasing RF power, and therefore it is not the reason for the increase in ion energy between 400 and 800 W. Given the complex interactions of the ion beam with the quasi-neutral downstream plasma, the power dependencies of the ion beam flux and energy are difficult to ascribe to any one effect. The FWHM of the IED (figure 15) is 4.3 eV and only slightly dependent of power, increasing a bit with increasing power, and saturating at $> 800$ W.

### 3.5. Dependences on bias phase and duration

The neutralization of the ion beam is expected to depend strongly on the relative fluxes of beam ions and cold plasma that pass through the extraction grid since the higher the flux of cold plasma the more electrons can be provided to neutralize the space charge of the ion beam. This ratio can be varied by changing the duration of the bias voltage and the delay between the ICP power and bias pulses.

Figure 16 shows RFEA measurements of ion beam current as a function of the delay between turn-off of the plasma power and application of DC bias to the boundary electrode. In all cases, the DC bias was turned off at $t = 95$ $\mu$s, so the bias duration decreases as the delay increases, as indicated on the upper *x*-axis of figure 16. The solid red line in the figure is the relative current expected for 20% duty cycle, using the data in figure 6 to compute the integrated current over the bias pulse. For delay times of 30 $\mu$s or more, the current measured at the RFEA is a constant fraction of the current emerging from the plasma source, meaning that the space charge neutralization
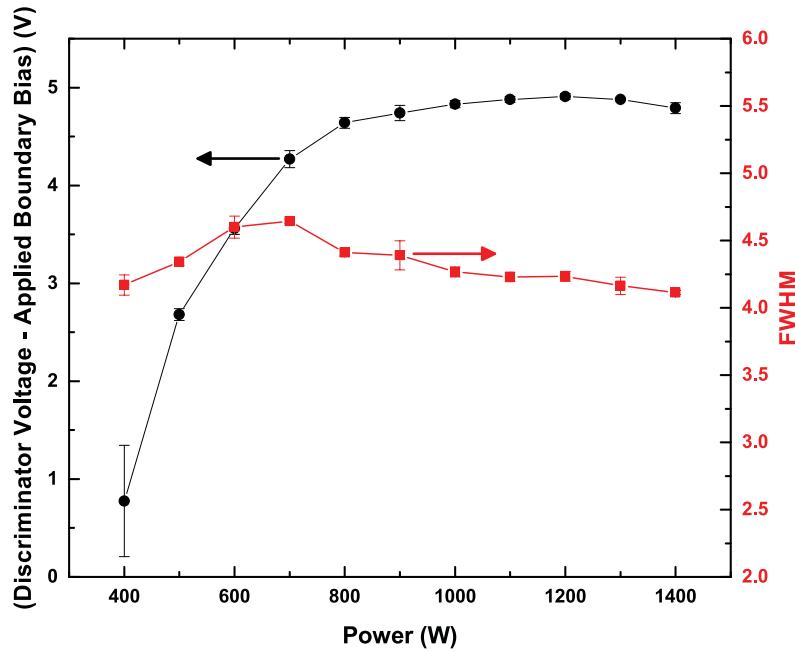
**Figure 15.** Peak ion energy above the applied bias and FWHM of the IED versus peak RF power to the ICP source. Other parameters were at their base case value.
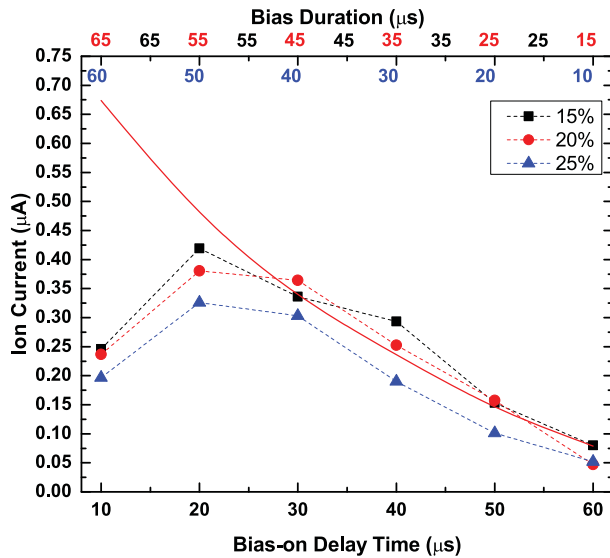


**Figure 16.** Ion current versus delay in applying the DC boundary bias in the afterglow, with respect to the end of the power pulse. Bias is turned off at 95 $\mu$s in all cases. Bias durations are given at the top of the figure for the duty cycles of 15% (black squares), 20% (red circles) and 25% (blue triangles). The solid red line is the relative ion current emerging from the plasma for the 20% duty cycle case. Otherwise, base conditions were used.

is optimized. If the delay time is too short ($<$30 $\mu$s) then not enough low-energy plasma is present adjacent to the grid to neutralize the ion beam space charge and the current falls.

Ion currents and energy distributions 80 cm from the extraction grid were also measured as a function of the duration of DC bias applied to the boundary electrode, for different duty cycles (figure 17). The delay between turn-off of plasma
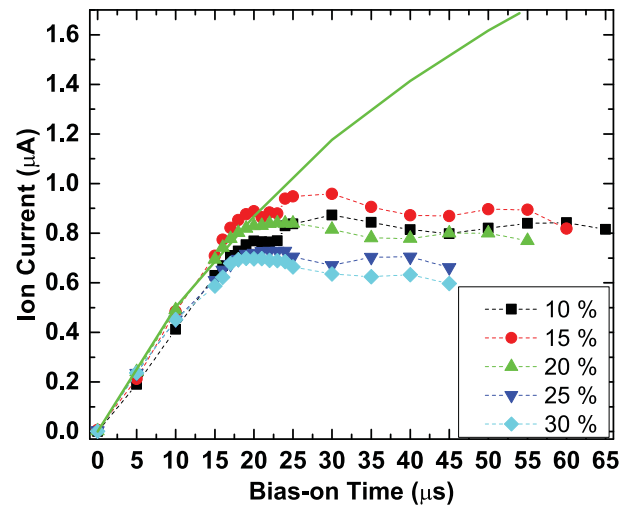


**Figure 17.** Ion current versus duration of the DC boundary bias applied in the afterglow, 20 $\mu$s after the ICP power was extinguished, for duty cycles of 10% to 30%. The solid green line is the relative ion current emerging from the plasma for the 20% duty cycle case. Otherwise, base conditions were used.

power and initiation of DC bias was fixed at 20 $\mu$s. Ion current increases linearly with increasing bias duration up to 15 $\mu$s, and then reaches saturation for a bias duration longer than 20 $\mu$s. The green solid line represents the relative ion current for the 100 eV beam that passes through the extraction grid for the 20% duty cycle case, extracted from the flux in figure 6, integrated over the bias durations. Apparently, at bias durations longer than 20 $\mu$s, there is no longer sufficient density of plasma in the downstream region of the grid to neutralize the space charge, and the ion current saturates.

## 4. Summary

A nearly monoenergetic $Ar^+$ ion beam, with self-neutralized space charge, was extracted from a power modulated (pulsed) inductively coupled plasma (ICP) through a single grounded grid. The beam energy was set by applying a synchronous DC bias voltage to a boundary electrode in contact with the plasma in the late afterglow of the power pulse. A retarding field energy analyzer (RFEA) and a movable Faraday cup were used to measure the ion energy distributions (IEDs) and the time resolved ion and electron currents, as a function of position along the beam axis, to unravel the mechanism of self-neutralization of the beam space charge.

The ion current contained a sharp peak, appearing shortly after the application of DC bias on the boundary electrode, corresponding to the nominal 100 eV ion beam, and a broad background appearing after plasma power was turned on, due to low energy ions that were either accelerated to the un-biased plasma potential ($\sim 5T_e$), or were produced by resonant charge exchange collisions of ions with background neutrals near the extraction grid. These slow ions in conjunction with periodic injection of electrons (mainly at the beginning of the afterglow) formed a plasma downstream of the extraction grid. Electrons from this background plasma were attracted by the passing high energy ion beam, neutralizing the beam space charge.

The ion current was found to drop drastically immediately downstream of the extraction grid (0–4 cm away) mainly due to charge exchange collisions. Farther away from the extraction grid, the rate of decay of ion current decreased and was eventually determined by the angular divergence of the ions. Beyond ~35 cm from the extraction grid, the electron current fell precipitously as the space charge was too low for ambipolar diffusion to contain the electrons.

The IED at a distance of 80 cm from the extraction grid was measured using the RFEA. The peak of the IED decreased monotonically as a function of pressure (5–35 mTorr), and it was ~2 eV above (at 5 mTorr) and ~3 eV below (at 35 mTorr) the nominal value of 100 eV. The IED also broadened with increasing pressure. The peak ion energy at 80 cm increased from 0.8 eV above the bias voltage at 400 W to 4.6 eV above the bias voltage at 800 W and then reached a plateau at ~4.8 eV above the bias voltage beyond 800 W. The dependence of ion current at 80 cm as a function of the time delay of the application of the DC bias suggested an optimum set of conditions for space charge neutralization.

## Acknowledgments

## Appendix A. Estimation of the time for the ion current to reach its peak value in figure 7

To obtain a better measure of the time the ion current reaches its peak value, the transit time of ions travelling from the extraction grid to the Faraday cup must be considered. Ions passing through the 3 grids on the Faraday cup will strike the current collector cup with a delay of the time it takes for ions to travel from the extraction grid to the second grid of the Faraday cup, and then strike the near end of the cylindrical wall of the current collector cup, plus the time it takes for ions to travel an additional ~7 cm to reach the flat surface of the current collector cup (see figure 3). Near the end of the power-on period, $T_e = 4.5$ eV, hence $v_D = 1.02 \times 10^6$ cm s$^{-1}$. Even with the angular distribution, it only takes ~0.2 $\mu$s to travel the 0.16 cm distance from the first to the second grid of the Faraday cup. The ions then either drift to the third grid (when the current collector is grounded), or are accelerated by the $-101$ V potential on the current collector cup, when the cup is biased to repel electrons. The transit times for ions to travel the 0.72 cm distance from grid 2 to grid 3 of the Faraday cup are ~1 or ~0.5 $\mu$s without or with the $-101$ V current collector bias, respectively. In the unbiased case, ions traveling at $1.02 \times 10^6$ cm s$^{-1}$ take an additional ~6.3 $\mu$s to travel 6.3 cm from the third grid to the flat surface of the current collector cup.

Therefore, the maximum delay time between entering the first grid and detection with no bias on the Faraday cup is about 7.5 $\mu$s, but since most ions will strike the cylindrical surface of the current collector cup, given the 18° angular spread, the delay time is probably closer to 5 $\mu$s. With bias on the Faraday cup, the velocity of ions is $3 \times 10^6$ cm s$^{-1}$ in the collector, so it takes only 2 $\mu$s to reach the flat surface at the back of the current collector cup. Since in this case the angular spread is much less, more ions are detected deeper into the collector and the total delay time is ~3 $\mu$s, i.e. only slightly different than the case with no bias. Given these estimates, it appears that the ion current in figure 7 peaks within 1 or 2 $\mu$s after the end of the power-on period.

## Appendix B. Effect of charge exchange collisions on the measured ion current

For an Ar plasma with an upstream pressure, $P$, the downstream pressure at the location of the grid was estimated to be $0.7P$. Charge exchange collisions in the sheath are negligible, hence all charge exchange occurs between the grid and the RFEA. The background pressure measured with a capacitance manometer 5 cm away from the grid was 0.23 mTorr for $P = 10$ mTorr, or in general $0.023P$. The background gas density will transition from nearly independent of distance from the grid over the first ~0.5 cm, to decreasing as the inverse square of distance at ~5 cm. If we roughly approximate this

J. Phys. D: Appl. Phys. 52 (2019) 355205

Y-M Chen et al

as a linear fall-off in number density, then we estimate that, given a charge exchange (dominant collision) cross section of $5 \times 10^{-15}$ cm$^2$ [28], the % transmission of the 100 eV beam through this near-grid region is 27%, 7%, 0.5% and 0.003% for pressure = 5, 10, 20, and 40 mTorr. Therefore, charge exchange is the major factor contributing to the initial drop in ion beam current.

## ORCID iDs

Ya-Ming Chen ⓘ https://orcid.org/0000-0002-0325-110X
Vincent M Donnelly ⓘ https://orcid.org/0000-0001-5834-6678
Demetre J Economou ⓘ https://orcid.org/0000-0001-6272-4862

## References

[1] Aisenberg S and Chabot R 1971 *J. Appl. Phys.* **42** 2953–8
[2] Conrad J R, Radtke J, Dodd R, Worzala F J and Tran N C 1987 *J. Appl. Phys.* **62** 4591–6
[3] Reyntjens S and Puers R 2001 *J. Micromech. Microeng.* **11** 287
[4] Asakawa K and Sugata S 1985 *J. Vac. Sci. Technol.* B **3** 402–5
[5] Smidt F 1990 *Int. Mater. Rev.* **35** 61–128
[6] Jahn R G 2006 *Physics of Electric Propulsion* (New York: Courier)
[7] Watt F, Bettiol A, Van Kan J, Teo E and Breese M 2005 *Int. J. Nanosci.* **4** 269–86
[8] Xu L, Nasrullah A, Chen Z, Jain M, Ruchhoeft P, Economou D J and Donnelly V M 2008 *Appl. Phys. Lett.* **92** 013124
[9] Xu L, Vemula S C, Jain M, Nam S K, Donnelly V M, Economou D J and Ruchhoeft P 2005 *Nano Lett.* **5** 2563–8
[10] Tian S 2015 *PhD Dissertation* University of Houston
[11] Harper J M E, Cuomo J J, Leary P A, Summa G M, Kaufman H R and Bresnock F J 1981 *J. Electrochem. Soc.* **128** 1077–83
[12] Brown I G 2004 *The Physics and Technology of Ion Sources* (New York: Wiley)
[13] Chang J P, Arnold J C, Zau G C H, Shin H-S and Sawin H H 1997 *J. Vac. Sci. Technol.* A **15** 1853–63
[14] Dudin S and Rafalskyi D 2009 *Europhys. Lett.* **88** 55002
[15] Rafalskyi D and Aanesland A 2014 *J. Phys. D: Appl. Phys.* **47** 495203
[16] Tian S, Donnelly V M and Economou D J 2015 *J. Vac. Sci. Technol.* B **33** 030602
[17] Xu L, Economou D J, Donnelly V M and Ruchhoeft P 2005 *Appl. Phys. Lett.* **87** 041502
[18] Tian S, Donnelly V M, Ruchhoeft P and Economou D J 2015 *Appl. Phys. Lett.* **107** 193109
[19] Liu L, Sridhar S, Zhu W, Donnelly V M, Economou D J, Logue M D and Kushner M J 2015 *J. Appl. Phys.* **118** 083303
[20] Liu L, Sridhar S, Donnelly V M and Economou D J 2015 *J. Phys. D: Appl. Phys.* **48** 485201
[21] Dudin S V, Rafalskyi D V and Zykov A V 2010 *Rev. Sci. Instrum.* **81** 083302
[22] Economou D J 2008 *J. Phys. D: Appl. Phys.* **41** 024001
[23] Kim C-K and Economou D J 2002 *J. Appl. Phys.* **91** 2594–603
[24] Kim C-K 2000 *PhD Dissertation* University of Houston
[25] Hara K, Kaganovich I D and Startsev E A 2018 *Phys. Plasmas* **25** 011609
[26] Soloshenko I 1996 *Rev. Sci. Instrum.* **67** 1646–52
[27] Kaganovich I, Davidson R, Dorf M, Startsev E, Sefkow A, Lee E and Friedman A 2010 *Phys. Plasmas* **17** 056703
[28] Lieberman M A and Lichtenberg A J 1994 *MRS Bull.* **30** 899–901
[29] Shin H, Zhu W, Xu L, Donnelly V M and Economou D J 2011 *Plasma Sources Sci. Technol.* **20** 055001